Photodissociation Dynamics of the Charge-Transfer State of the $C_6H_6-I_2$ Complex

Gary DeBoer, Joseph W. Burnett, Akira Fujimoto,† and Mark A. Young*

Department of Chemistry, University of Iowa, Iowa City, Iowa 52242

Received: May 17, 1996; In Final Form: June 24, 1996[⊗]

A pulsed-extraction time-of-flight method was employed to investigate the photodissociation dynamics of the $C_6H_6-I_2$ charge-transfer state. Measurement of the kinetic energy release for the I atom fragments indicates that the charge-transfer state dissociates to a $I(^2P_{3/2}) + I^*(^2P_{1/2})$ product state. An anisotropic high-velocity distribution and a Maxwell−Boltzmann distribution with a velocity-dependent spatial anisotropy were observed as distinct components in the product spectra. Rapid dissociation from an oblique complex geometry, with the I_2 bond axis inclined at an angle with respect to the benzene symmetry axis, appears to be responsible for the experimental results. The free I atom recoils away from the complex while the bound I atom interacts strongly with the benzene partner, yielding the different fragment distributions. As a result of charge-transfer excitation, the I_2 is left on the same repulsive excited state that is optically accessed in the uncomplexed molecule, leading to prompt fragmentation. A second mechanism, producing slow I atom fragments, may also contribute to the Maxwell−Boltzmann component. The $C_6H_6-I_2$ complex manifests behavior that can only be understood on the basis of the entire supramolecular complex while other aspects can be rationalized from characteristics of the separated fragments.

Introduction

A number of investigators have recently capitalized on the manifold advantages afforded by photofragment translational spectroscopy to investigate the dynamics of chemical reactions occurring in the confines of a weakly bound cluster or complex.[1−12] The nearly universal applicability of the method, and the ability to accurately determine the kinetic energy release (KER), make it especially useful in cluster-based reactions where a range of product fragments in different final states is often produced. The resultant spectra are found to be extremely sensitive to various aspects of the cluster environment, such as the cluster geometry and details of the intermolecular potential. As has been pointed out,[13,14] chemical reactions in oriented complexes can probe reactive and nonreactive potential energy surfaces in a highly specific manner. In the current article, we report initial results from our studies of the KER in $C_6H_6-I_2$ complexes utilizing a pulsed-extraction time-of-flight (TOF) method.

We have previously applied the method to the study of relatively weakly bound systems, such as small $(HI)_n$ clusters.[8] The intermolecular interactions in these systems, and other similar species, are dominated by weak H-bonding and dispersion forces. Chemical reactions can often be understood on the basis of slightly modified gas phase potentials while taking into account the restricted range of impact parameters. An interesting contrast might be provided by molecular complexes that undergo a charge-transfer (CT) process upon excitation. While often weakly interacting in the ground state, CT excitation leads to much stronger, ionic-type attraction due to the transfer of charge from the donor species to the acceptor species. The CT mechanism depends on intimate overlap of donor−acceptor molecular orbitals and the excitation is, thus, characteristic of the whole complex as opposed to localized excitation of an individual chromophore. Subsequent chemical processes may also be more unique to the complex than the atom−molecule reactions that have previously been studied in bound complexes.

We have begun to investigate various candidate CT systems to serve as a counterpoint to our work with more weakly interacting systems. We have initially focused on the prototypical CT complex, $C_6H_6-I_2$, a system with a long history dating back to the first observations of CT phenomena by Benesi and Hildebrand[15,16] and the theoretical explanations provided by Mulliken.[17,18] There have been a number of pertinent studies of the dynamics of CT excitation in iodine−arene complexes in the liquid phase using ultrafast probe techniques.[19−23] Recently, Zewail and collaborators conducted experiments on the $C_6H_6-I_2$ CT complex isolated in a supersonic expansion.[10,11] These comprehensive experiments coupled femtosecond time-resolved methods with measurements of KER in the product fragments. It was possible to monitor the growth of the I atom fragment in real time and make comparisons to the dynamics in uncomplexed I_2.

We have investigated the KER of I atom fragments resulting from excitation of the CT state in $C_6H_6-I_2$ complexes using a TOF analysis. We detect both ground state $I(^2P_{3/2})$ and spin−orbit excited $I^*(^2P_{1/2})$ as product species. The spectrum for either product species contains two distinct fragment translational energy distributions, exhibiting very different characteristics, but both can be associated with CT excitation. One component is peaked at a high velocity and retains a significant spatial anisotropy while the other is Maxwell−Boltzmann-like and displays a velocity-dependent anisotropy. The differences can be ascribed to the initial geometry of the photoexcited CT complex and subsequent rapid dynamics. Facile fragmentation appears to occur from an electronically excited state of I_2 populated by the CT process. Other insights into the gas phase behavior of the $C_6H_6-I_2$ complex are possible from considerations of the data.

Experimental Section

We have previously provided details regarding the instrument used to collect the TOF spectra in these experiments.[8] A commercial pulsed valve is the source for a supersonic expansion which generates the $C_6H_6-I_2$ complexes. A He stream, maintained at a stagnation pressure of 30 psig for all of the

† Permanent address: Department of Materials Science and Engineering, Tokyo Denki University, Tokyo 101, Japan.

[⊗] Abstract published in *Advance ACS Abstracts,* August 15, 1996.

S0022-3654(96)01430-X CCC: $12.00

results reported here, passes through a stainless steel bubbler containing benzene. The vapor pressure of benzene in the He buffer is controlled by maintaining the temperature of the bubbler with either a dry ice/solvent bath or an immersion cooler. Iodine crystals are held in a small reservoir just behind the pulsed valve solenoid assembly, yielding a vapor pressure of ≈0.3 Torr for all of our experiments. The expansion is skimmed, and the collimated beam is transmitted to the extraction region of a reflectron time-of-flight mass spectrometer (RTOFMS).

Absorbing species are excited, and product fragments photoionized, within a single laser pulse in a one-color experiment. An excimer−pumped dye laser combination is used to generate the requisite tunable UV radiation, separated from the fundamental by a prism assembly. The CT absorption of $C_6H_6-I_2$ has a long wavelength limit of around 305−315 nm and a maximum at approximately 268 nm, as measured in the gas phase.[24,25] After a search for suitable transitions, we have chosen to probe ground state $I(^2P_{3/2})$ atoms at 265.91 nm, corresponding to a 2 +1 resonance enhanced multiphoton ionization (REMPI) process through the 7p ($^2D_{5/2}$) state. Spin−orbit excited $I^*(^2P_{1/2})$ atoms were probed at 277.32 nm through the 8p ($^2P_{1/2}$) state. Both probe wavelengths lie well within the $C_6H_6-I_2$ CT band. Efficient polarization of the probe laser beam was ensured by the placement of a Glan-Focault polarizer inside the dye laser. Information concerning polarization dependence was obtained by the use of a double Fresnel−Rhomb (Karl Lambrecht Corp.) to rotate the incident laser polarization. The polarization orientation could be varied continuously but was usually fixed to be either parallel to the collection axis of the RTOFMS (defined as $\alpha = 0°$) or perpendicular to the axis ($\alpha = 90°$).

Any resultant photoions are allowed to drift under field-free conditions for a fixed delay before being extracted by a HV pulse applied to the repeller electrode of the RTOFMS. The flight time of the ions is then related to the nascent KER by the spatial distribution of the fragments prior to application of the HV pulse. The flight time spectra are transformed to a laboratory frame velocity distribution according to

$$I^{\alpha}(v_z) = f^{\alpha}(\mathrm{TOF})\frac{\mathrm{d(TOF)}}{\mathrm{d}(v_z)} \qquad (1)$$

where v_z, the projection of the velocity vector onto the collection axis of the instrument, is determined from a nonlinear solution of the known TOF equations for our instrument. The $I^{\alpha}(v_z)$ can then be related to the fragment recoil speed distribution, $g(v)$, by

$$I^{\alpha}(v_z) = \int_{v_{\min}}^{v_{\max}} \frac{g(v)}{2v}\left[1 + \beta P_2(\cos\alpha) P_2\left(\frac{v_z}{v}\right)\right] \mathrm{d}v \qquad (2)$$

where α is the laser polarization angle with respect to the collection axis of the instrument and β is the spatial anisotropy parameter which, in general, may be expressed as a function of the velocity, $\beta(v_z)$. The integral is evaluated over the range $v_{\min} = |v_z|$ to $v_{\max} = (v_z^2 + v_d^2)^{1/2}$. The detection sensitivity for velocity components perpendicular to the collection axis is determined by v_d, the discrimination velocity. A small value of v_d allows the measured v_z to closely approach the recoil velocity, v, and results in core sampling conditions, as has been described by Hwang and El-Sayed.[26] The resolution of our instrument was improved from previous work by the addition of a 5 mm diameter aperture to the entrance grid of the microchannel plate detector. The actual value of v_d is somewhat larger than calculated due to the blurring effect of grids in the ion extraction optics.[12] The value for our experimental configuration, $v_d \approx 120$ m/s, corresponding to an effective aperture diameter of ≈9 mm, was determined from calibration measurements.

In the limit of large KER, where $v \gg v_d$, core sampling conditions are relevant and the integral of eq 2 can be approximated as

$$I^{\alpha}(v_z) = \frac{g(v)}{4}[1 + \beta P_2(\cos\alpha)]\frac{v_d^2}{v_z^2} \qquad (3)$$

Thus, for core sampling, the measured $I^{\alpha}(v_z)$ can be scaled as

$$I^{\alpha}(v_z)v_z^2 \propto g(v) \qquad (4)$$

to directly yield the form of the recoil speed distribution, as has been discussed by Syage.[12] If $g(v)$ is described by a Maxwell−Boltzmann function, with an isotropic spatial distribution ($\beta = 0$), the same scaling holds regardless of the relative magnitude of the recoil velocity.[12] The only difference between these two cases is the proportionality constant needed in eq 4.

In the $C_6H_6-I_2$ photofragmentation experiments, there are clearly several overlapping distributions present in the spectra. Unfortunately, the scaling relation of eq 4 cannot unravel the different contributions. An approximate separation of the various components was achieved by assuming an analytical form for each $g(v)$ and then numerically evaluating the integral of eq 2. The sum of the calculated distributions was then compared to the experimental spectrum. We have assumed that $g(v)$ can be represented by either a Gaussian function, described by a peak velocity and a full width at half-maximum (fwhm), or a Maxwell−Boltzmann function, characterized by a rms velocity. The calculated distributions were convoluted with an instrument response function previously determined from calibration studies. The amplitudes of the various calculated distributions were then scaled to fit the measured data. These scaling factors can be corrected for the velocity and angle-dependent detection sensitivity to obtain the actual relative intensities.

Results

Mass-resolved spectra were recorded with the RTOFMS operating in its normal mode with a continuous extraction voltage applied to the ionization region. Mass spectra for two different benzene vapor pressures are shown in Figure 1. The probe laser was fixed at 262.8 nm, a nominal wavelength chosen for nonresonant photoionization conditions. At this wavelength, the two-photon energy (9.43 eV) lies just above the ionization potentials (IP) of C_6H_6 (9.247 eV) and I_2 (9.3995 eV). For either vapor pressure, a series of benzene clusters, $(C_6H_6)_n^+$, are clearly observed as the dominant mass signal. However, we also observe small signals corresponding to $(C_6H_6)_2-I^+$ and $C_6H_6-I^+$ in the higher pressure spectrum, but the former mass peak is barely detectable in the lower pressure spectrum. No parent ions of the type $(C_6H_6)_n-(I_2)_m^+$ were observed. In contrast, the femtosecond excitation source used by Zewail and coworkers[10,11] led to easily detectable signals from unfragmented parent ions. Clearly, rapid dynamics must occur upon excitation of $C_6H_6-I_2$ species at these wavelengths.

We have also monitored, under similar excitation conditions, the intensity of some of the mass signals as a function of the benzene vapor pressure, and the results are presented in the form of a log−log plot in Figure 2. The I^+ and I_2^+ signals increase slightly with increasing benzene vapor pressure but then rapidly decrease at pressures above approximately 1−2 Torr. Below 8 Torr of benzene vapor, the $C_6H_6-I^+$ and $(C_6H_6)_2-I^+$ signals

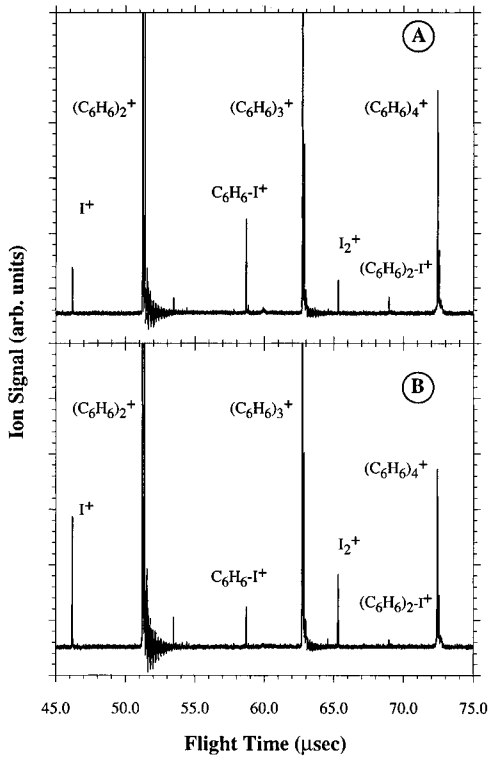

Figure 1. Mass spectra obtained for I_2/C_6H_6/He expansions with benzene vapor pressures of 23.7 Torr (A) and 8.0 Torr (B).

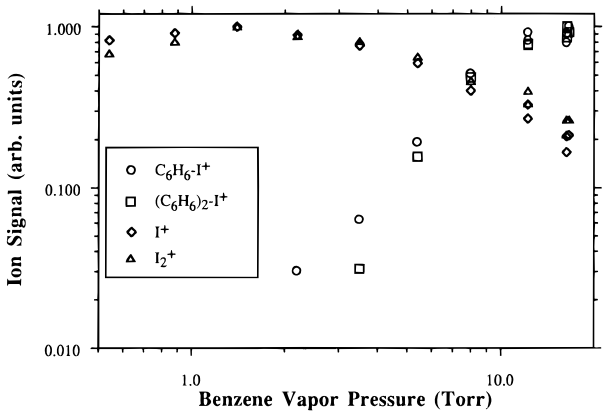

Figure 2. A log−log plot of the benzene vapor pressure dependence of various mass signals.

exhibit different low-pressure slopes with values of approximately 2 and 3, respectively. The last pressure for which the $C_6H_6-I^+$ signal was recorded appears to indicate that the slope is becoming even more shallow. No mass signals corresponding to mixed clusters of benzene and iodine were observed below vapor pressures of about 2 Torr.

The flight time spectra for I and I* photofragments were recorded at 265.91 and 277.32 nm, respectively, corresponding to excitation within the $C_6H_6-I_2$ CT absorption band. In the absence of benzene, only relatively weak I^+ signals were observed, presumably the result of I_2 photofragmentation at these wavelengths. However, upon addition of trace benzene vapor to the gas stream, an increased I^+ signal was observed and with a much different kinetic energy signature. These fragments are associated with photoprocesses induced by excitation of $C_6H_6-I_2$ cluster species. In Figure 3 we present flight time spectra for the I* fragment collected with laser polarizations of $\alpha = 0°$ and 90° and with a benzene vapor pressure of 0.8 Torr. Cursory examination of the spectra reveal that several distinct velocity distributions must contribute to the observed data. A peaked,

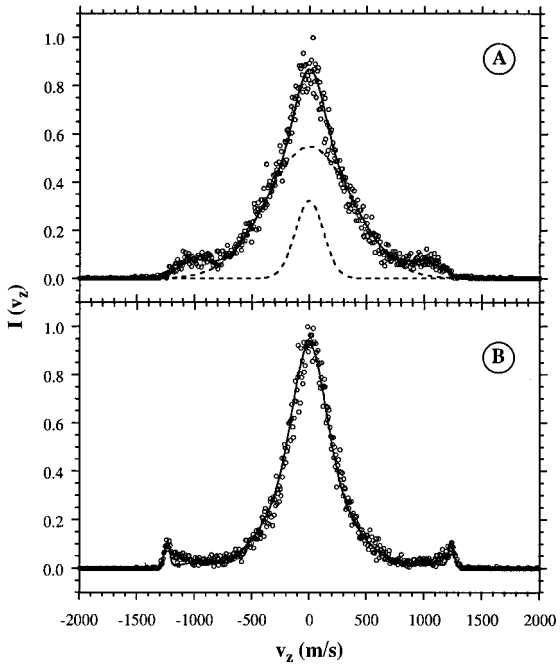

Figure 3. I*($^2P_{1/2}$) photofragment velocity spectra obtained with a benzene vapor pressure of 0.8 Torr. The probe laser is oriented either parallel, $\alpha = 0°$ (A), or perpendicular, $\alpha = 90°$ (B), to the collection axis of the instrument. The solid line represents a calculated fit using the parameters listed in Table 1. In (A), the two Maxwell−Boltzmann functions used to fit the central feature are also depicted separately by dotted lines.

high-velocity component is present in the $\alpha = 0°$ spectrum but exhibits a greatly reduced intensity when the laser is rotated to $\alpha = 90°$, indicating a degree of spatial anisotropy in the photofragmentation process. A Gaussian function centered at 1050 ± 20 m/s and with a fwhm of 325 ± 20 m/s was used to fit these fragments, as summarized in Table 1. The anisotropy parameter of the distribution was determined to be $\beta = 1.0 \pm 0.1$, which represents an average result from several similar spectra.

A broad component, peaked at zero velocity in the laboratory frame, is quite prominent and appears to be relatively isotropic. While the spectra suggest a simple Maxwell−Boltzmann type distribution, the data was not well described by a single function. However, it was possible to fit the results at either polarization with a sum of two Maxwell−Boltzmann distributions; a relatively hot component and a colder component (Table 1). The cold component makes a readily discernible contribution to the laboratory frame distribution, even though it is actually an order of magnitude less intense than the hot component, because of the enhanced sensitivity of the TOF method to slow velocity fragments relative to faster species. The effect is illustrated in Figure 3A which separately depicts the two Maxwell−Boltzmann components for the $\alpha = 0°$ data.

The shape of the central Maxwell−Boltzmann feature clearly changes upon rotation of the laser polarization, indicating a residual spatial anisotropy that is velocity dependent. Such behavior indicates that the separation of the angular and speed parts of the photofragment distribution implied by eq 2 is not exactly valid in the cluster environment due to collisional effects. The polarization data can be used to calculate the anisotropy parameter, β, as a function of velocity via the relationship

$$\beta(v_z) = \frac{I^{0°}(v_z) - I^{90°}(v_z)}{0.5I^{0°}(v_z) + I^{90°}(v_z)} \qquad (5)$$

TABLE 1: Parameters Used To Fit the Photofragment Speed Distributions Observed in the Experimental $I^{\alpha}(v_z)$ Spectra and the Mean Translational Energies, $\bar{E}_{t,c.m.}$, Calculated for Each Distribution

fragment	α (deg)	function	peak/rms velocity (m/s)	fwhm (m/s)	β	parent	$\bar{E}_{t,c.m.}$ (cm^{-1})[b]
$I^*(^2P_{1/2})$	0	Maxwell−Boltzmann[a]					
		hot (0.63)	638 ± 10				
				c	0	$C_6H_6-I_2$	2799 ± 100
		cold (0.37)	209 ± 10				
		Gaussian	1050 ± 20	325 ± 20	1.0 ± 0.1	$C_6H_6-I_2$	9643 ± 360
	90	Maxwell−Boltzmann[a]					
		hot (0.42)	557 ± 10				
				c	0	$C_6H_6-I_2$	2799 ± 100
		cold (0.58)	235 ± 10				
		Gaussian	1050 ± 20	325 ± 20	1.0 ± 0.1	$C_6H_6-I_2$	9643 ± 360
		Gaussian	1240 ± 10	20	−1	I_2	16326 ± 260
$I(^2P_{3/2})$	0	Maxwell−Boltzmann[a]					
		hot (0.67)	718 ± 10				
				c	0	$C_6H_6-I_2$	3704 ± 115
		cold (0.33)	267 ± 10				
		Gaussian	1110 ± 20	360 ± 20	1.0 ± 0.1	$C_6H_6-I_2$	10794 ± 380
	90	Maxwell−Boltzmann[a]					
		hot (0.44)	621 ± 10				
				c	0	$C_6H_6-I_2$	3704 ± 115
		cold (0.56)	238 ± 10				
		Gaussian	1110 ± 20	360 ± 20	1.0 ± 0.1	$C_6H_6-I_2$	10794 ± 380
		Gaussian	1295 ± 10	20	−1	I_2	17807 ± 275

[a] The relative intensity of each Maxwell−Boltzmann function used to fit the experimental $I^{\alpha}(v_z)$ data is given in parentheses. [b] The mean energy for the Maxwell−Boltzmann component was determined from a calculated magic-angle speed distribution. [c] Not applicable.

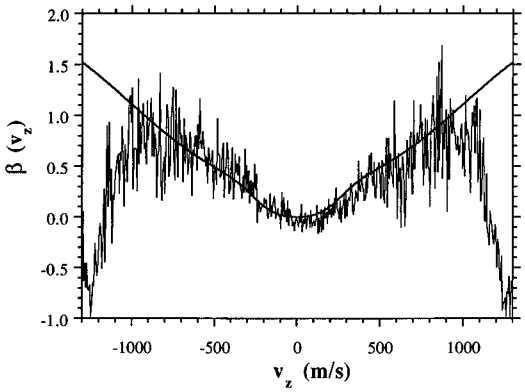

Figure 4. Plot of the velocity dependence of the anisotropy parameter, $\beta(v_z)$, for the experimental data of Figure 3 for the I* product channel. The solid line is the result calculated from the fit to the central velocity feature seen in Figure 3.

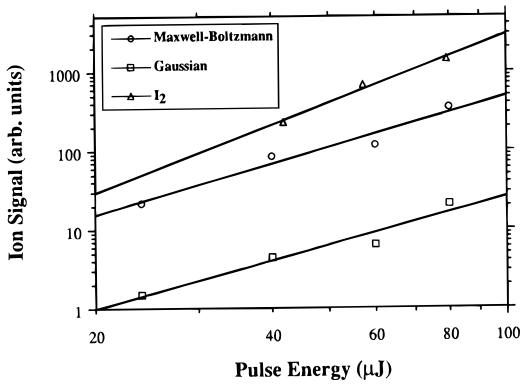

Figure 5. A log−log plot of the probe laser intensity dependence of the Gaussian and Maxwell−Boltzmann fragment distributions due to cluster excitation observed in Figure 3. The data for both distributions have a slope of approximately 2.0 ± 0.3, as indicated by the straight lines. The intensity dependence of the distribution derived from bare I_2 photodissociation is also included and was determined to have a slope of approximately 2.9 ± 0.3.

The resultant plot is shown in Figure 4 along with the calculated $\beta(v_z)$ from the Maxwell−Boltzmann fit to the central feature. As can be seen from Figure 4, the higher velocity fragments exhibit an increasingly positive value for the anisotropy parameter, appearing to approach a limiting value of $\beta \approx 1.0$.

The $\alpha = 90°$ data (Figure 3B) shows a relatively narrow feature peaked at even higher velocities which was fit to a Gaussian function with the parameters contained in Table 1. The component has a large, negative β value, as displayed in the $\beta(v_z)$ plot of Figure 4, that is close to the value for a pure perpendicular transition, −1.0. These features persist, with approximately the same intensity, in the absence of benzene and also exhibit a different power dependence (Figure 5) from the other spectral features. Thus, the fragment distribution is confidently assigned to uncomplexed I_2 species present in the supersonic expansion. The translational energy release, E_t, expected for I_2 photodissociation can be calculated from energy conservation

$$E_t = h\nu + E_{int}^{p} - D_0^0(I_2) - E_{so} \qquad (6)$$

where $h\nu$ is the photon energy, E_{int}^{p} is the internal energy of the parent, $D_0^0(I_2)$ is the I_2 bond energy (1.542 eV), and E_{so} is the spin−orbit energy of iodine (0.943 eV). The calculated energy with the inclusion of spin−orbit excitation agrees well with our experimental results, indicating that fragmentation yields I and I* as products.

In order to help ascertain whether the Maxwell−Boltzmann distribution and the high velocity, anisotropic Gaussian distribution have their origins in the same excitation process, we conducted a laser intensity dependence study at the I* probe wavelength. The number of data points was constrained by the necessity for long signal averaging. The results, shown in the log−log plot of Figure 5, indicate that both components have quadratic intensity dependence, with slopes of 2.0 ± 0.3, in the laser energy regime measured. Figure 5 also contains the relevant data for the intensity dependence of the fragment distribution assigned to bare I_2 photodissociation. A slope of approximately 2.9 ± 0.3 was empirically determined.

We have also investigated the ground-state I atom fragment channel by probing at 265.91 nm and the relevant data for both $\alpha = 0°$ and 90° are shown in Figure 6. The resultant spectra are analogous to those obtained for the I* channel and,

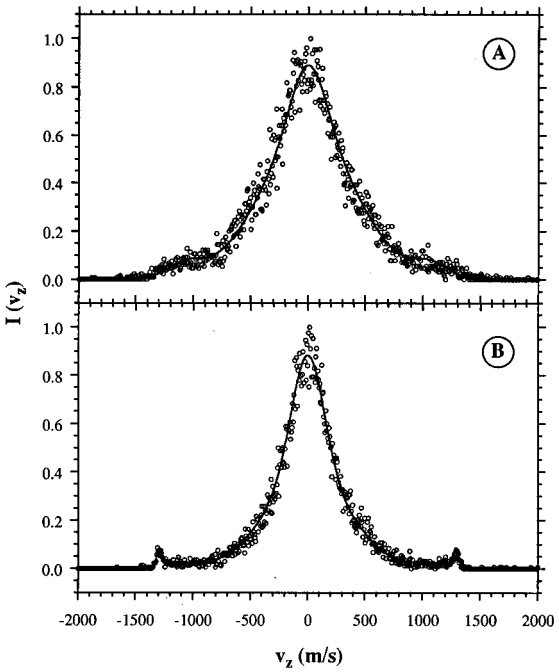

Figure 6. I($^2P_{3/2}$) photofragment velocity spectra obtained with a benzene vapor pressure of 0.8 Torr. The probe laser is oriented either parallel, $\alpha = 0°$ (A), or perpendicular, $\alpha = 90°$ (B), to the collection axis of the instrument. The solid line represents a calculated fit using the parameters listed in Table 1.

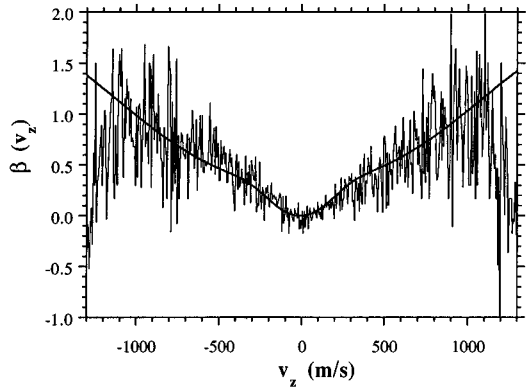

Figure 7. Plot of the velocity dependence of the anisotropy parameter, $\beta(v_z)$, for the experimental data of Figure 6 for the I product channel. The solid line is the result calculated from the fit to the central velocity feature seen in Figure 6.

consequently, the fitting parameters were determined to be similar (Table 1) although a larger KER is indicated. Of particular interest is the observation that the bare I_2 photofragment distribution has a roughly similar relative intensity in both the I and I* flight time spectra. The velocity dependence of the anisotropy parameter, $\beta(v_z)$, is determined from eq 5 and plotted in Figure 7 along with the calculated results from the fit to the central Maxwell−Boltzmann distribution.

We measured the flight time spectra at slightly higher benzene vapor pressures, about 4.8 Torr, conditions which yielded both $C_6H_6-I^+$ and $(C_6H_6)_2-I^+$ signals in the mass spectrum. The $I^\alpha(v_z)$ distributions were qualitatively similar although the details of the fitting parameters for the Maxwell−Boltzmann feature were slightly different, tending to be somewhat colder (smaller values of the rms velocity). However, between 2.0 and 0.3 Torr, the lowest benzene vapor pressure that could be examined, the experimental spectra and the requisite fitting parameters did not change appreciably. We also examined the spectra as a function of the laser excitation energy to determine whether space charge effects may plague the interpretation. Over the range of pulse energies employed, 20−120 μJ, no systematic changes in the appearance of the spectra or the value of the fitting parameters were detected. The flight time spectra displayed here were recorded with relatively low pulse energies, 40−60 μJ, to ensure that no such effects skewed the observations.

The fitting parameters used to describe the data are summarized in Table 1. In the case of the Maxwell−Boltzmann feature the fragment speed distribution, $g^\alpha(v)$, is dependent on the polarization angle, as we have noted (vide supra). Thus, to facilitate comparison with the other components, a magic angle distribution ($\alpha = 54.74°$), $g^M(v)$, was obtained from

$$g^M(v) = {}^1/_3(g^{0°}(v) + 2g^{90°}(v)) \qquad (7)$$

corresponding to an angle-averaged speed distribution.

Discussion

In the experiments of Zewail and co-workers on $C_6H_6-I_2$ complexes in a supersonic expansion,[10,11] the most prominent feature in the reported mass spectrum is a progression of $(C_6H_6)_n-I_2^+$ cluster species. The 275 nm excitation wavelength used in these studies lies below the two-photon threshold for ionization of uncomplexed C_6H_6. Their femtosecond laser source is capable of yielding multiphoton absorption rates that can effectively compete with parallel fragmentation pathways. In contrast, under similar expansion conditions, we have observed only relatively weak signals due to fragment ions, such as $C_6H_6-I^+$, and no parent ion signals could be detected. The more modest multiphoton excitation rates afforded by our nanosecond laser source apparently cannot overcome rapid fragmentation of the complex induced by absorption at these wavelengths. Zewail and co-workers measured the transient appearance of the I^+ fragment in real time and found a time constant of 750 fs, corresponding to a fragmentation rate on the order of 10^{12} s^{-1}. In condensed phase studies of the mesitylene$-I_2$ CT complex, dissociation of the iodine bond was determined to occur in no more than 25 fs,[20,21] an order of magnitude faster. We crudely estimate our ionization rate to be on the order of $(8-10) \times 10^7$ s^{-1} for the pulse energies and focusing conditions used in obtaining the mass spectral data so it is not surprising that the parent ions are difficult to detect.

The mass spectra of Figure 1 were collected with an excitation energy that is only about 50 cm^{-1} below the vibronic origin of the C_6H_6 $\tilde{A}$ $^1B_{2u}$ state. Weakly interacting van der Waals (vdW) complexes of aromatic species often exhibit small red shifts in the aromatic electronic absorption spectrum. A similar shift is expected for the $C_6H_6-I_2$ vdW complex, perhaps as large as 60−70 cm^{-1} in analogy with the red shift in toluene−Xe,[27] and it is possible that the observed dynamics originate in excitation of the benzene chromophore. However, the flight time spectra recorded for the I and I* fragmentation channels utilized excitation energies that are 490 and 2037 cm^{-1} below the benzene $\tilde{A}$ $^1B_{2u}$ origin, respectively. The KER for these two fragment channels is similar in appearance (Figures 3 and 6), suggesting a common mechanism that does not involve localized benzene excitation. The I_2 absorption cross section is very small at these UV wavelengths, on the order of 10^{-20} cm^2.[28,29] The different laser intensity dependence measured for the I atom fragments of bare I_2 dissociation compared to those resulting from clusters (Figure 5) also suggest that the iodine chromophore is an unlikely excitation pathway.

We propose, then, that the observed behavior is due to excitation of the $C_6H_6-I_2$ CT state which is an absorption characteristic of the entire supramolecule rather than a localized

excitation of one of the complexed species. The CT band is broad and extends to wavelengths, approximately 305−315 nm in the gas phase, that encompass those used in the current studies. Subsequent dynamics, as expressed in the measured KER for the fragment species, originate from the transfer of an electron from a donor benzene molecular orbital to an acceptor orbital localized on the I_2 molecule.

It is clear from the mass-resolved spectra (Figure 1) that larger $(C_6H_6)_n-I_2$ clusters are present in the expansion at higher benzene vapor pressures. The yield of I^+ and I_2^+ is also observed to decay as the benzene vapor pressure is increased. The mechanism for the observed decrease in these mass signals is not yet clear. If the larger clusters form structures that are effective in inhibiting I_2 fragmentation via solvent cage effects, then it is possible that the resultant I_2 product is produced with a degree of internal excitation that reduces the photoionization yield. Considerable vibrational excitation of the caged I_2 fragments has been detected for excitation of $(C_6H_6)_n-I_2$ clusters at longer wavelengths, in the vicinity of 480 nm.[30] It will be interesting to investigate the partitioning of excess energy into the I_2 internal degrees of freedom for larger clusters, similar to our previous experiments on the products of $(HI)_n$ cluster photodissociation.[31]

At pressures below about 8 Torr of benzene vapor, the $C_6H_6-I^+$ and $(C_6H_6)_2-I^+$ mass signals have slopes of approximately 2 and 3, respectively, in the log−log plot of Figure 2. Such a dependence on benzene pressure suggests that these $(C_6H_6)_n-I^+$ species are fragment ions from $n + 1$ parent clusters. However, the slope of the $C_6H_6-I^+$ signal appears to be decreasing over the last two pressures for which signal could be obtained. Below about 2.0 Torr, no $(C_6H_6)_n-I^+$ ions could be detected. The KER data reported here was collected at a much lower benzene pressure of 0.8 Torr. In addition, at pressures less than 2 Torr no discernible changes were evident in the KER of I atom fragments associated with cluster formation. Under these rarefied sample conditions we propose that we have reached limiting behavior and that the dominent species in the expansion is the dimer complex, $C_6H_6-I_2$. For approximately the same beam conditions, Zewail and co-workers observed that $C_6H_6-I_2^+$ was the predominant parent ion in their mass spectra.[10,11]

We have transformed the fitted fragment speed distributions, $g(v)$, for each distinct component observed in the experimental I atom flight time spectra to a center-of-mass (c.m.) translational energy distribution, $P(E_{t,c.m.})$, according to

$$P(E_{t,c.m.}) = \frac{g(v)}{v}\left(\frac{m_P - m_I}{m_I m_P}\right) \tag{8}$$

where the c.m. translational energy is given by

$$E_{t,c.m.} = \frac{m_I v^2}{2}\left(\frac{m_P}{m_P - m_I}\right) \tag{9}$$

and m_I is the I atom fragment mass and m_P is the mass of the parent species. In accordance with the arguments presented, we have assumed that the appropriate parent mass is that of the $C_6H_6-I_2$ dimer complex for the fragments that derive from CT excitation. We have also performed the appropriate transformation for the component due to uncomplexed I_2 photofragmentation for comparison. All of the calculated $P(E_{t,c.m.})$ for the I and I* channels are collected in Figure 8, and the mean translational energy, $\bar{E}_{t,c.m.}$, for each distribution is listed in Table 1. The integrated area of each distribution approximately

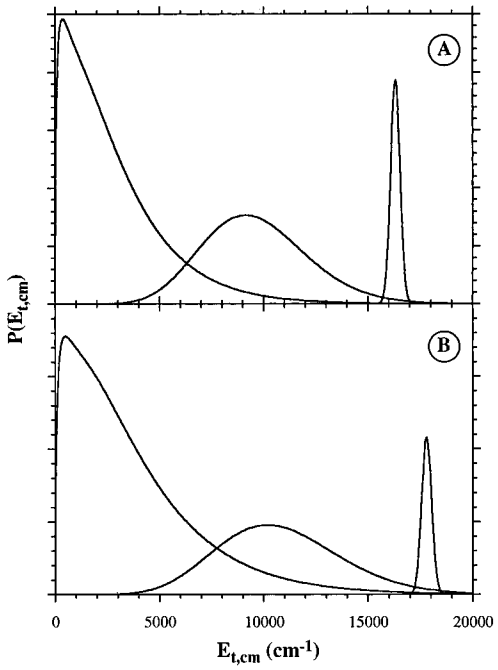

Figure 8. Translational energy distributions, $P(E_{t,c.m.})$, for the two components resulting from excitation of the $C_6H_6-I_2$ CT state when the I* (A) or I (B) product fragment is probed. The $P(E_{t,c.m.})$ for uncomplexed I_2, the sharp distribution peaked at high energies, is also included and is scaled by a factor of 0.5.

corresponds to its actual relative probability, after correcting for the angle- and velocity-dependent detection sensitivity.

Two distinct fragment $P(E_{t,c.m.})$ distributions result from dissociation of the $C_6H_6-I_2$ complex; a higher energy Gaussian distribution and a Maxwell−Boltzmann distribution. These two features have the same laser intensity dependence and the same dependence on the benzene vapor pressure. We tentatively conclude that they are different products resulting from the same excitation mechanism. These fragment species display a quadratic laser intensity dependence while the analogous I atom fragments of molecular iodine decomposition exhibit a cubic dependence (Figure 5). As the MPI process is the same for the free I atom fragments regardless of the source, the difference in the intensity dependence suggests that the CT transition is saturated. From a consideration of the laser flux required for saturation, we estimate the $C_6H_6-I_2$ CT absorption cross section to be $\sigma \approx (3-8) \times 10^{-18}$ cm^2, which is in approximate agreement with vapor phase measurements of $\sigma \approx (2-3) \times 10^{-18}$ cm^2 calculated from difference spectra.[24,25] Excitation of I_2 at the UV wavelengths used in our study is thought to be due to the $^3\Sigma_{1u}^+$ state, a component of the C state continuum, which dissociates to form I + I* through a perpendicular transition.[32−34] The KER and anisotropy parameter, $\beta = -1$, measured from our data are consistent with such an interpretation. CT excitation of the $C_6H_6-I_2$ complex also yields I and I* as product species (Figures 3 and 6). The $P(E_{t,c.m.})$ for bare I_2 photofragmentation has approximately the same relative probability whether the I or the I* product is probed (Figure 8). In addition, the fragment distributions derived from the $C_6H_6-I_2$ complex have the same general appearance regardless of which I atom product is examined. The ratio of the mean translational energies for the Gaussian I and I* fragment distributions is

$$\bar{E}^{I}_{t,c.m.}/\bar{E}^{I*}_{t,c.m.} = 1.12$$

From eq 6, the ratio of the excess energy available at the

different I atom probe wavelengths is about 1.10 when the iodine spin−orbit energy is included, very close to the experimental value for the Gaussian distribution. The release of the I* spin−orbit energy (0.943 eV) would be easily discerned. The implication, then, is that the I and I* fragments correlate with the same asymptotic product state and are produced in the same fragmentation process,

$$C_6H_6{-}I_2 \xrightarrow{h\nu} C_6H_6 + I + I^* \qquad (10)$$

In addition, there does not appear to be significant quenching of the spin−orbit excited I* via interactions within the complex for the fragments giving rise to the Gaussian product distribution. The $P(E_{t,c.m.})$ for the bare I_2 photofragments in Figure 8 provide an indication of the total energy available from the dissociation pathway of eq 10, assuming that the I_2 bond energy is unchanged upon complexation and neglecting the binding energy of the ground-state complex.

If the fragmentation mechanism is a simultaneous three-body process, as may be the situation for the reaction described by eq 10, then the transformation is not so straightforward. Measurement of the individual fragment velocities will not uniquely determine the total translational energy, as is the case for a two-body process. However, a sequential fragmentation mechanism would make the simple transformation valid for the primary photofragment, which is probably a reasonable assumption for the anisotropic, Gaussian velocity component.[35,36] The resultant $P(E_{t,c.m.})$ obtained from eqs 8 and 9 may be considered as approximate but are useful for further discussion regarding the dynamics of the CT complex.

While the two complex fragment distributions apparently derive from excitation of the CT state, the obvious differences in the spatial and speed distributions indicate that they experience different dynamics subsequent to excitation. A possible source for the observed differences is an initial geometry of the $C_6H_6{-}I_2$ complex that entails inequivalent I atoms. In our previous work with $(HI)_n$ species, the I atom flight time spectra was broad and isotropic, resembling the Maxwell−Boltzmann distribution observed for I atom fragments in the current experiments. We ascribed the previous results to cage effects for I atom fragments of HI photodissociation within a cluster.[8] In contrast, we have examined systems such as $C_2H_2{-}HI$ and $C_6H_6{-}HI$, where the binding is between the acidic hydrogen and the π-electron system to give a "T"-shaped complex with a free I atom.[37] In these systems, the I atom KER was virtually unchanged from monomer dissociation and cage effects are not evident. Other investigators have discussed similar relationships between the geometry of a complex and the observed angle−velocity distribution of product fragments.[7,12,38] The Gaussian I atom distribution we have measured for $C_6H_6{-}I_2$ fragmentation is peaked at a high energy and is anisotropic. We therefore associate this distribution with a free, nonbinding I atom in the parent complex. The Maxwell−Boltzmann distribution is more characteristic of a fragment that has undergone cage type interactions upon dissociation and we therefore associate these species with bound I atoms in the parent $C_6H_6{-}I_2$ complex. The velocity dependence of the anisotropy is reflective of the dynamics of escape from the solvent "cage" induced by complexation. Other effects may give rise to the resultant differences in the fragment distributions, but the above discussion provides a logical basis for further analysis.

The equilibrium structure of the $C_6H_6{-}I_2$ complex has not been definitively determined. Vibrational spectra of matrix isolated $C_6H_6{-}I_2$ complexes,[39] ab initio[20,40] and semiempirical calculations,[30,41,42] as well as consideration of electrostatic

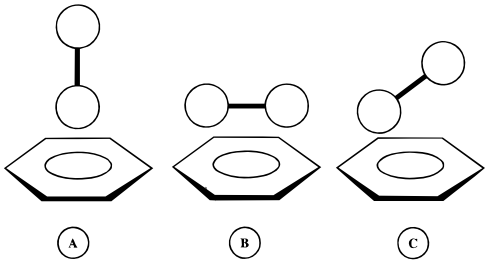

Figure 9. Three proposed structures for the $C_6H_6{-}I_2$ complex: axial (A), resting (B), and oblique (C).

interactions[43,44] all suggest that the I_2 molecule is aligned with the C_6 axis of benzene, as shown in Figure 9A. Crystal structures of the $C_6H_6{-}Cl_2$ and $C_6H_6{-}Br_2$ 1:1 compounds have been determined from X-ray diffraction data and also place the molecular halogen perpendicular to the aromatic plane.[45,46] However, similar matrix isolation IR investigations of these latter complexes, along with the $C_6H_6{-}ICl$ species, concluded that the structure is oblique with the halogen bond axis tilted away from the perpendicular.[47] Mulliken originally analyzed the $C_6H_6{-}I_2$ complex in terms of a "resting" structure, with the I_2 bond axis oriented parallel to the plane of the ring, but later reasoned that an oblique or axial arrangement was also possible from considerations of CT stabilization of the ground state complex.[18] Theoretical treatments[20,30,40−42] have generally found the resting structure to be less stable than the axial arrangement although the respective energies may be quite close. The oblique and resting configurations for $C_6H_6{-}I_2$ are also depicted in Figure 9.

We can analyze our experimental results in terms of each of these complex structures. A similar analysis has been applied to studies of I_2−arene CT complexes in the condensed phase.[22] The $C_6H_6{-}I_2$ complex is weakly interacting, with a binding energy of approximately 750 cm^{-1} for the axial configuration,[20,30] and will undergo large-amplitude intermolecular motions as a consequence. However, in the low-temperature environment of the supersonic expansion, we expect the structure of the complex to be relatively well defined, unlike the liquid phase situation. Such an interpretation is consistent with the cryogenic matrix studies of aromatic−halogen complexes where, for instance, interconversion between isomeric structures does not occur.[47] Molecular dynamics simulations also predict that only the axial $C_6H_6{-}I_2$ structure is present at low temperatures, <50 K, but that a distribution of configurations exists at higher temperatures.[42]

The CT interaction requires that there be nonzero overlap between the donor and acceptor molecular orbitals (i.e., they must have the same irreducible representation in the point group of the complex) with a benzene π orbital as the donor and an iodine σ^* orbital as the acceptor. In the axial configuration, the σ^* orbital has maximum overlap with the lower energy a_{2u} π orbital of benzene, both of which are a_1 in C_{6v} symmetry. In addition, the higher IP of the a_{2u} orbital would place the CT transition at much shorter wavelengths than we have utilized in the current study. We can estimate the CT excitation energy, E_{CT}, from the ionization potential of the donor, the electron affinity of the acceptor (EA), and the approximate distance between the charge centers in the complex, R_{DA},

$$E_{CT} = IP - EA - e^2/R_{DA} \qquad (11)$$

The IP of the a_{2u} orbital is 12.2 eV,[48] and the EA of I_2 is 2.5 eV.[49] Using the spacing between the planes of graphite, 3.5 Å, to approximate the extent of the C_6H_6 π-orbitals and the Lennard-Jones parameter for I_2, $\sigma = 4.98$ Å,[50] we estimate, R_{DA}

$\approx$ 4.2 Å. The predicted CT energy is then 6.3 eV (197 nm), well above the energy of the probe laser.

The axial structure has two inequivalent I atoms, which is in accordance with our interpretation of the experimental observations, but the CT transition moment would be parallel to the I_2 bond axis. We might then expect to observe an anisotropy parameter closer to the limiting value of 2.0 rather than the reduced value ($\beta \approx 1.0$) we have empirically determined for the free I atom. However, as we discuss below, the presence of large-amplitude bending motions in an axial complex may serve to reduce the measured β from the limiting value.

In the resting configuration, which has C_{2v} symmetry, the σ^* orbital is either of b_1 or b_2 symmetry, depending on the orientation of the I_2 bond axis. Nonzero overlap with the degenerate benzene e_{1g} orbitals is possible in C_{2v} symmetry since these reduce to the appropriate b_1 and b_2 representations. However, this structure has two equivalent I atoms and is inconsistent with our interpretation of the observed KER. In addition, the CT transition moment is perpendicular to the I_2 bond axis and would manifest a negative anisotropy parameter, perhaps near the limiting value of -1. We experimentally measure a positive anisotropy parameter. Thus, it does not appear that $C_6H_6-I_2$ complexes in the resting geometry can contribute to the observed CT state dynamics.

In the oblique configuration, the symmetry is reduced to C_s and both benzene π bonding orbitals have nonzero overlap with the I_2 σ^* orbital and can contribute to the CT interaction, which would lower the transition energy. The IP of the benzene e_{1g} orbital, 9.25 eV, would put the CT state at $\approx$3.35 eV, according to eq 11, and is consistent with our probe laser energy. In addition, the lower symmetry would allow mixing with localized benzene $\pi-\pi^*$ excitation, such as the nearby $^1B_{2u}-{}^1A_{1g}$ transition, which would enhance the intensity of the CT band.[51,52] The CT transition moment would be in the symmetry plane, which contains the I_2 bond axis and is perpendicular to the aromatic ring plane.

The oblique structure would be consistent with our experimental observations in that the I atoms are inequivalent. The free I atom would be able to escape the complex with minimal interference from cage effects, producing the Gaussian distribution seen in the fragment spectrum. However, the Gaussian $P(E_{t,c.m.})$ still peaks at a lower energy than that of the bare I_2 photofragment and is very broad, indicating that there are still consequences of the CT complex environment. The I atom directed toward the ring would interact strongly with the benzene complex partner upon I_2 fragmentation, yielding the observed Maxwell−Boltzmann distribution. It is possible that a relatively long-lived C_6H_6-I collision complex is formed. It is known that excitation of the I_2−aromatic CT band in solution leads to the production of a transient I atom complex[21,23,53] and photochemical iodination reactions due to CT excitation have also been observed.[54] We previously invoked the role of a collision complex to explain the presence of slow H atoms in the photofragment spectra of $(HI)_n$ clusters.[8] The subsequent decay of such a transient could lead to the velocity dependence of the anisotropy parameter, especially if rotational excitation is present due to fragmentation in an oblique geometry.

There may also be evidence for quenching of the $I^*(^2P_{1/2})$ spin−orbit energy due to collisions with the benzene since the $\bar{E}_{t,c.m.}$ for the Maxwell−Boltzmann distribution obtained by monitoring the $I(^2P_{3/2})$ product is larger than expected simply on the basis of the shorter wavelength probe. In our previous studies of $(HI)_n$ cluster photofragmentation we detected no significant change in the I/I* branching.[8] However, TOF investigations of the spin−orbit branching in small clusters of CH_3I did note marked changes relative to the monomer.[12,38] Photodecomposition of thin films of CH_3I deposited on metal surfaces also led to a substantial degree of quenching, ascribed to an external heavy atom effect.[55]

The measured rapid dissociation of the iodine bond,[10,11,20,21] coupled with the possible formation of a relatively long-lived collision complex between the "caged" I atom and benzene, lends credence to the view that the dissociation process follows a sequential mechanism and provides some justification for the assumptions discussed in obtaining the $P(E_{t,c.m.})$. The fact that the high-energy tail of $P(E_{t,c.m.})$ for the Gaussian distribution (Figure 8) approximately coincides with the energy release from the pathway of eq 10 provides further support for such a view.

Further insight into the structure of the CT complex is possible from a careful consideration of the experimentally measured anisotropy parameter. As we have mentioned, the somewhat low value of β indicated by the data may be the result of motions within the weakly bound complex. Simons and co-workers concluded, on the basis of their attempts to model the observed band shape of the $C_6H_6-I_2$ CT absorption in the condensed phase, that bending modes of the complex must play an important role.[52,56] In the axial geometry, a large-amplitude bending mode would introduce an angle between the transition dipole moment and the free I atom recoil velocity vector (corresponding to the I_2 bond axis). The anisotropy parameter is then given by

$$\beta = 2\int_{-\pi/2}^{+\pi/2} P_2(\cos\theta)\, P(\theta)\, \mathrm{d}\theta \qquad (12)$$

where θ is the angle between the transition moment and the recoil velocity vector, and $P(\theta)$ is the vibrational amplitude function for the bending mode. The value of β will be reduced as a consequence of the recoil distribution. As an example, we assume a totally flat potential between the axial ($\theta = 0$) and resting ($\theta = \pm\pi/2$) orientations so that the bend coordinate can be modeled with a square well potential. The amplitude function is then approximately described as, $P(\theta) \propto \cos^2\theta$. The anisotropy parameter would be reduced from the limiting value to about 1.2 in this example, still appreciably larger than the measured result. It may be more realistic to make a comparison with the bending modes of the C_6H_6-Ar complex, which exhibits a rms amplitude of about 5°,[57] or C_2H_2-HCl,[58] which displays an amplitude of about 9°. The very weakly bound $He-I_2$ complex may have a zero-point bending amplitude as large as 20°.[59] Mean amplitudes on the order of 10° would only decrease the value of β to about 1.9.

The above discussion would seem to indicate that intermolecular vibrations alone cannot account for the low β value we have determined. The remaining, alternative explanation is that excitation of oblique $C_6H_6-I_2$ complexes is responsible for the observed CT state dynamics. Assuming a rms deviation of about 5−10° in the bend coordinate, we estimate the angle between the aromatic C_6 axis and the I_2 bond axis to be $\theta \approx$ 35°. Ultrafast pump−probe experiments on various CT systems in the condensed phase have also detected an initial polarization anisotropy that is determined by the geometry of the complex.[21,22] For instance, in the mesitylene$-I_2$ system an angle of 45° was measured, not so different from our value.[21] However, more extensive studies reveal that the anisotropy is critically dependent on the nature of the solvent[22] and comparisons with condensed phase behavior are not so facile in this case. Wiersma and co-workers used semiempirical methods to calculate the oscillator strength of the CT transition as a function of the bending angle in the $C_6H_6-I_2$ complex and found a maximum at $\theta \approx 30°$, in good agreement with our experimental

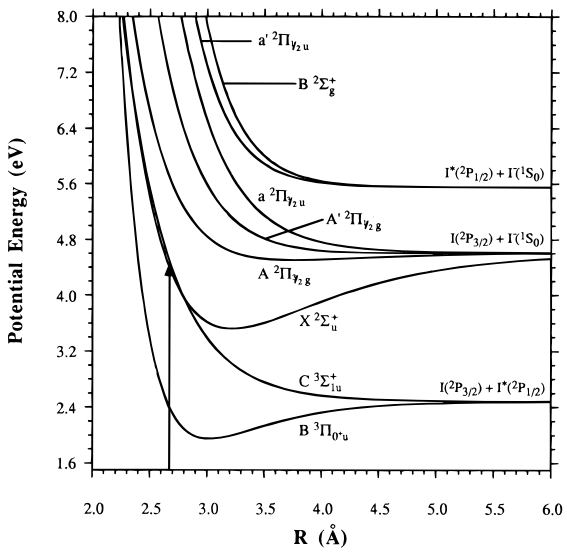

Figure 10. Potential energy curves for I_2^- (from ref 61), shifted by E_{CT}, and potentials for the B and C states of the neutral molecule.

results.[20] The calculated transition dipole moment was mainly directed from the center of the ring to the I_2 center of mass, as we have assumed for the oblique complex. They also concluded, on the basis of ab initio investigations, that the axial geometry is the most stable, but CT excitation preferentially occurs from bent configurations due to the distribution of geometric configurations present in the room temperature liquid environment.

Photofragmentation of the CT complex in the oblique configuration is likely to lead to considerable rotational excitation in the benzene fragment due to the impulsive recoil of the I atom. The analogous situation for CT complexes of mesitylene$-I_2$ in the condensed phase has been discussed, although the extent of rotational excitation was not directly measured.[20,21] We have conducted preliminary wavelength-resolved experiments to assess the disposition of excess energy into internal degrees of freedom and have detected considerable rotational energy in the C_6H_6 fragment, as expected.[60]

In Figure 10 we have reproduced the potential curves[61] for I_2^- where the energy scale has been shifted in accordance with E_{CT} calculated from eq 11. The vertical arrow represents the energy of the probe laser photon for I*, positioned at the neutral I_2 bond length, $R_{eq} = 2.67$ Å. These anionic potentials are instructive but only approximate since they will surely be modified in the CT complex.[62] We have also included two excited state potentials for the neutral species, the B $^3\Pi_{0^+u}$ state and the C $^3\Sigma_{1u}^+$ state.[32] At the probe energy used, it is unlikely that any excited states of I_2^- are accessible and, depending on the exact value of E_{CT}, it appears that only bound, or barely dissociative, states of the X $^2\Sigma_u^+$ potential can be reached in a vertical transition. In contrast, thermal electron attachment to neutral gas phase I_2 populates the repulsive $^2\Pi_g$ state.[63] In some earlier time-resolved studies of the $C_6H_6-I_2$ complex in the condensed phase, the observed rapid dissociation was interpreted on the basis of population of the $^2\Pi_g$ state by the CT process.[23]

We have proposed that excitation of the CT state correlates with a product asymptote yielding I and I*. Since such a pathway is not available on an anionic potential, the system must dissociate on a neutral curve. The logical candidate for the neutral potential is the state optically accessed in bare I_2, the C $^3\Sigma_{1u}^+$ state, as diagrammed in Figure 10. The exact shape of the C state potential in the complex is uncertain, but it is probably near the relevant anionic potential at our probe energies. One way to view the overall process is as a series of fast charge-transfer steps followed by dissociation

$$C_6H_6-I_2 \xrightarrow{h\nu} C_6H_6^+-I_2^- \rightarrow C_6H_6-I_2^* \rightarrow C_6H_6 + I + I^* \quad (13)$$

The electronic configuration for the ground state I_2^- species is $\sigma_g^2\pi_u^4\pi_g^4\sigma_u^1$ while the configuration of the C $^3\Sigma_{1u}^+$ state of the neutral is $\sigma_g^1\pi_u^4\pi_g^4\sigma_u^1$. Thus, the charge-recombination step would involve a different orbital than the original acceptor orbital in the photoinduced CT process. Barbara and collaborators, in their studies of halogen atom$-$arene complexes, have demonstrated the critical nature of the donor$-$acceptor geometry in the kinetics of charge recombination.[64,65] For the $C_6H_6-I_2$ structures we have considered (vide supra), the σ_g and σ_u orbitals of I_2 will have the same symmetry and can interact similarly with the benzene π-orbitals, facilitating rapid charge recombination. Sension and co-workers have also outlined an analogous mechanism to explain the fast dynamics they have measured for CT excitation of mesitylene$-I_2$ complexes in the condensed phase.[19] It is interesting that despite the supramolecular nature of the $C_6H_6-I_2$ CT complex, some aspects of the photodissociation dynamics can still be understood on the basis of the isolated I_2 species.

Zewail and collaborators have identified another mechanism that may contribute to the lower energy Maxwell$-$Boltzmann photofragment distribution that we have observed.[10,11] They have reasoned, from the results of femtosecond laser experiments, that the major route for fragmentation of the $C_6H_6-I_2$ complex is through a harpoon mechanism

$$C_6H_6\cdots I_2 \xrightarrow{h\nu} C_6H_6^+\cdots I_2^- \rightarrow C_6H_6^+\cdots I^-\cdots I \rightarrow C_6H_6^+\cdots I^- + I \quad (14)$$

with only a small amount of energy appearing in translational modes of the primary products. The relatively long-lived $C_6H_6^+-I^-$ intermediate can then dissociate through either radiative or nonradiative processes, such as charge recombination,[64,65] to form secondary I atoms. Consideration of the integrated areas of the $P(E_{t,c.m.})$ distributions in Figure 8 allows us to estimate that the harpoon mechanism could account for approximately 30$-$40% of the complex fragment species detected in our experiments. Any such mechanism would also have to rationalize the formation of I($^2P_{3/2}$) and spin$-$orbit excited I*($^2P_{1/2}$) atoms since a similar Maxwell$-$Boltzmann distribution is observed for both product species. If, indeed, CT excitation leads to a 2:1 branching ratio between reactions 13 and 14, then our data would suggest that different final product states of the harpoon reaction yield I and I*. However, only a fraction of the available excess energy for any product state resides in translational degrees of freedom. Further elucidation of the form of the relevant potential energy surfaces is certainly desirable. As has been discussed,[19] the I_2^- potentials will be perturbed in the presence of a charged benzene molecule. Calculations indicate that even very modest electric fields will make the $I + I^-$ product state isoenergetic with the zero-point of I_2^-, creating a barrier to dissociation.[62]

Conclusion

We have employed a pulsed-extraction TOF method to investigate the kinetic energy release upon excitation of the CT state in the $C_6H_6-I_2$ complex. We observe two distinct I atom fragment distributions which reflect the initial geometry of the CT complex; a higher energy, anisotropic distribution and a Maxwell$-$Boltzmann distribution that is relatively isotropic.

From considerations of the various possibilities, we conclude that an oblique geometry with the I_2 bond axis inclined at an angle of about 35° with respect to the C_6 axis of benzene is the most likely structure. The oblique structure is characterized by inequivalent I atoms. The free I atom recoil velocity vector is directed away from the complex while trajectories for the bound I atom lead to interactions with the benzene complex partner, perhaps forming a relatively long-lived collision complex. The net effect of CT excitation is to leave the molecular iodine on an excited potential which then rapidly dissociates to produce I and spin−orbit excited I* as product fragments. The excited I_2 potential is likely the same state populated by optical excitation in the bare molecule, the $C\,^3\Sigma_{1u}^+$ state, and so the dynamics of the CT complex can, at least in part, be rationalized from considerations of the isolated constituents. A second process, perhaps a previously characterized harpoon mechanism,[10,11] may make a substantial contribution to the low-energy Maxwell−Boltzmann product distribution, accounting for about 30−40% of all the detected photofragments. In future work, we will endeavor to study the internal energy content of the benzene fragment using wavelength-resolved probes. The benzene product is likely to be rotationally excited, as confirmed by preliminary studies,[60] due to impulsive recoil in an oblique geometry.[20,21] The $C_6H_6-I_2$ CT complex is clearly a rich system to study photodissociation dynamics in a complex and provides an instructive contrast to the behavior of more weakly bound systems.

Note Added in Proof. We have learned that Zewail and co-workers will present very relevant results concerning their work on the C_6H_6-I_2 CT complex.[66]

Acknowledgment. Support from the Carver Scientific Research Fund is gratefully acknowledged.

References and Notes

(1) Hoffbauer, M. A.; Liu, K.; Giese, C. F.; Gentry, W. R. *J. Chem. Phys.* **1983**, *78*, 5567.
(2) Loo, R. O.; Hall, G. E.; Haerri, H.-P.; Houston, P. L. *J. Phys. Chem.* **1988**, *92*, 5.
(3) Loo, R. O.; Haerri, H.-P.; Hall, G. E.; Houston, P. L. *J. Chem. Phys.* **1989**, *90*, 4222.
(4) Penn, S. M.; Hayden, C. C.; Muyskens, K. J. C.; Crim, F. F. *J. Chem. Phys.* **1988**, *89*, 2909.
(5) Jaques, C.; Valachovic, L.; Ionov, S.; Bohmer, E.; Wen, Y.; Segall, J.; Wittig, C. *J. Chem. Soc., Faraday Trans.* **1993**, *89*, 1419.
(6) Segall, J.; Wen, Y.; Singer, R.; Wittig, C.; Garcia-Vela, A.; Gerber, R. B. *Chem. Phys. Lett.* **1993**, *207*, 504.
(7) Zhang, J.; Dulligan, M.; Segall, J.; Wen, Y.; Wittig, C. *J. Phys. Chem.* **1995**, *99*, 13680.
(8) Young, M. A. *J. Chem. Phys.* **1995**, *102*, 7925.
(9) Cheng, P. Y.; Zhong, D.; Zewail, A. H. *J. Phys. Chem.* **1995**, *99*, 15733.
(10) Cheng, P. Y.; Zhong, D.; Zewail, A. H. *Chem. Phys. Lett.* **1995**, *242*, 369.
(11) Cheng, P. Y.; Zhong, D.; Zewail, A. H. *J. Chem. Phys.* **1995**, *103*, 5153.
(12) Syage, J. A. *Chem. Phys. Lett.* **1995**, *245*, 605.
(13) Wittig, C.; Engel, Y. M.; Levine, R. D. *Chem. Phys. Lett.* **1988**, *153*, 411.
(14) Shin, S. K.; Chen, Y.; Oh, D.; Wittig, C. *Philos. Trans. R. Soc. London A* **1990**, *332*, 361.
(15) Benesi, H. A.; Hildebrand, J. H. *J. Am. Chem. Soc.* **1949**, *71*, 2703.
(16) Benesi, H. A.; Hildebrand, J. H. *J. Am. Chem. Soc.* **1948**, *70*, 3978.
(17) Mulliken, R. S. *J. Am. Chem. Soc.* **1950**, *72*, 600.
(18) Mulliken, R. S.; Person, W. B. *Molecular Complexes*; Wiley-Interscience: New York, 1969; p 171.
(19) Pullen, S.; II, L. A. W.; Sension, R. J. *J. Chem. Phys.* **1995**, *103*, 7877.
(20) Lenderink, E.; Duppen, K.; Everdij, F. P. X.; Mavri, J.; Torre, R.; Wiersma, D. A. *J. Phys. Chem.* **1996**, *100*, 7822.
(21) Lenderink, E.; Duppen, K.; Wiersma, D. A. *Chem. Phys. Lett.* **1993**, *211*, 503.
(22) Walker, L. A.; Pullen, S.; Donovan, B.; Sension, R. J. *Chem. Phys. Lett.* **1995**, *242*, 177.
(23) Hilinski, E. F.; Rentzepis, P. M. *J. Am. Chem. Soc.* **1985**, *107*, 5907.
(24) Lang, F. T.; Strong, R. L. *J. Am. Chem. Soc.* **1965**, *87*, 2345.
(25) Duerksen, W. K.; Tamres, M. *J. Am. Chem. Soc.* **1968**, *90*, 1379.
(26) Hwang, H. J.; Griffiths, J.; El-Sayed, M. A. *Int. J. Mass Spectrom. Ion Processes* **1994**, *131*, 265.
(27) Mons, M.; Calve, J. L.; Piuzzi, F.; Dimicoli, I. *J. Chem. Phys.* **1990**, *92*, 2155.
(28) Tamres, M.; Duerksen, W. K.; Goodenow, J. M. *J. Phys. Chem.* **1968**, *72*, 966.
(29) Passchier, A. A.; Gregory, N. W. *J. Phys. Chem.* **1968**, *72*, 2697.
(30) McLean, T. D.; Ratcliff, B. B.; Pastalan, J. Z.; Innes, K. K. *J. Quant. Spectrosc. Radiat. Transfer* **1989**, *42*, 445.
(31) Burnett, J.; Young, M. A. *Chem. Phys. Lett.* **1994**, *228*, 403.
(32) Mulliken, R. S. *J. Chem. Phys.* **1971**, *55*, 288.
(33) Clear, R. D.; Wilson, K. R. *J. Mol. Spectrosc.* **1973**, *47*, 39.
(34) Hwang, H. J.; El-Sayed, M. A. *J. Phys. Chem.* **1991**, *95*, 8044.
(35) Kroeger, P. M.; Riley, S. J. *J. Chem. Phys.* **1979**, *70*, 3863.
(36) Kroeger, P. M.; Riley, S. J. *J. Chem. Phys.* **1977**, *67*, 4483.
(37) DeBoer, G.; Burnett, J. W.; Young, M. A., unpublished results.
(38) Syage, J. A. *Chem. Phys.* **1996**, *207*, 411.
(39) Fredin, L.; Nelander, B. *J. Am. Chem. Soc.* **1974**, *96*, 1672.
(40) Kochanski, E.; Prissette, J. *Nouv. J. Chim.* **1980**, *4*, 509.
(41) Jano, I. *Theor. Chim. Acta* **1985**, *66*, 341.
(42) Danten, Y.; Guillot, B.; Guissani, Y. *J. Chem. Phys.* **1992**, *96*, 3782.
(43) Hanna, M. W. *J. Am. Chem. Soc.* **1968**, *90*, 285.
(44) Lippert, J. L.; Hanna, M. W.; Trotter, P. J. *J. Am. Chem. Soc.* **1969**, *91*, 4035.
(45) Hassel, O.; Stromme, K. O. *Acta Chem. Scand.* **1959**, *13*, 1781.
(46) Hassel, O.; Stromme, K. O. *Acta Chem. Scand.* **1958**, *12*, 1146.
(47) Fredin, L.; Nelander, B. *Mol. Phys.* **1974**, *27*, 885.
(48) Rosenstock, H. M.; Draxl, K.; Steiner, B. W.; Herron, J. T. *J. Phys. Chem. Ref. Data* **1977**, *6* (Suppl. 1).
(49) Lias, S. G.; Bartmess, J. E.; Liebman, J. F.; Holmes, J. L.; Levin, R. D.; Mallard, W. G. *J. Phys. Chem. Ref. Data* **1988**, *17* (Suppl. 1).
(50) Hirschfelder, J. O.; Curtiss, C. F.; Bird, R. B. *Molecular Theory of Gases and Liquids*; John Wiley and Sons: New York, 1954; p 1110.
(51) Murrell, J. N. *J. Am. Chem. Soc.* **1959**, *81*, 5037.
(52) McHale, J.; Banerjee, A.; Simons, J. *J. Chem. Phys.* **1978**, *69*, 1406.
(53) Strong, R. L. *J. Phys. Chem.* **1962**, *66*, 2423.
(54) Cozzens, R. F. *J. Phys. Chem.* **1975**, *79*, 18.
(55) Jensen, E. T.; Polanyi, J. C. *J. Phys. Chem.* **1993**, *97*, 2257.
(56) McHale, J.; Simons, J. *J. Chem. Phys.* **1979**, *70*, 4974.
(57) Maxton, P. M.; Schaeffer, M. W.; Ohline, S. M.; Kim, W.; Venturo, V. A.; Felker, P. M. *J. Chem. Phys.* **1994**, *101*, 8391.
(58) Lee, R.; Henderson, G. *J. Chem. Phys.* **1984**, *81*, 5521.
(59) Horn, T. R.; Gerber, R. B.; Ratner, M. A. *J. Chem. Phys.* **1989**, *91*, 1813.
(60) DeBoer, G.; Burnett, J. W.; Young, M. A. *Chem. Phys. Lett.*, in press.
(61) Chen, E. C. M.; Wentworth, W. E. *J. Phys. Chem.* **1985**, *89*, 4099.
(62) Maslen, P. E.; Papanikolas, J. M.; Faeder, J.; Parson, R.; ONeil, S. V. *J. Chem. Phys.* **1994**, *101*, 5731.
(63) Ayala, J. A.; Wentworth, W. E.; Chen, E. C. M. *J. Phys. Chem.* **1981**, *85*, 768.
(64) Jarzeba, W.; Thakur, K.; Hormann, A.; Barbara, P. F. *J. Phys. Chem.* **1995**, *99*, 2016.
(65) Hormann, A.; Jarzeba, W.; Barbara, P. F. *J. Phys. Chem.* **1995**, *99*, 2006.
(66) Cheng, P. Y.; Zhong, D.; Zewail, A. H. *J. Chem. Phys.*, in press.

JP9614308